PAPER

Proton transport in oxalate compounds of iron(III) containing (alkyl)ammonium cations: the influence of the density of hydrogen bonds on conductivity†

Ana Lozančić, [iD] Sanja Burazer, [iD] Sanja Renka, Krešimir Molčanov, [iD] Lidija Molčanov [iD] and Marijana Jurić [iD]*

The proton conduction behaviour of novel oxalate-based compounds of iron(III) of different nuclearity with various ammonium components, $(NH_4)_2[Fe(H_2O)Cl_3(C_2O_4)]\cdot H_2O$ (1), $\{[NH(CH_3)_2(C_2H_5)][FeCl_2(C_2O_4)]\cdot H_2O\}_n$ (2) and $\{[N(CH_3)(C_2H_5)_3][FeCl_2(C_2O_4)]\}_n$ (3), was investigated by impedance spectroscopy in addition to characterization by single-crystal and powder X-ray diffraction and infrared spectroscopy. The discrete mononuclear compound 1 exhibits a very high proton conductivity of 2.17×10^{-3} $(\Omega \text{ cm})^{-1}$ at 25 °C and 74% relative humidity (RH), with σ_{DC} increased by nearly seven orders of magnitude. The three-dimensional (3D) hydrogen-bonding network of NH_4^+ cations and water molecules (crystal and coordinated) as hydrogen-bond donors and the bidentate oxalate ligand and chloride ions of the anionic moiety $[Fe(H_2O)Cl_3(C_2O_4)]^{2-}$ as hydrogen-bond acceptors plays a crucial role in proton transport; the density of the formed hydrogen-bonds positively impacts the mobility of protons in the nonporous structure of 1. The one-dimensional (1D) compounds 2 and 3, both containing infinite anionic zig-zag chains $[FeCl_2(C_2O_4)]_n^{n-}$ and cations $(CH_3)_2(C_2H_5)NH^+$ (2) or $(CH_3)(C_2H_5)_3N^+$ (3), showed an increase in conductivity of six and five orders of magnitude, reaching values of 2.00×10^{-4} $(\Omega \text{ cm})^{-1}$ and 9.17×10^{-6} $(\Omega \text{ cm})^{-1}$, respectively, at 25 °C and 93% RH. Compared to compound 3, compound 2 has hydrogen-bonded protonated $(CH_3)_2(C_2H_5)NH^+$ cations that exhibit greater hydrophilicity, which is closely related to the affinity for water molecules that significantly affect proton transport and conductivity.

Introduction

Proton conductivity has been studied as a novel functionality of metal–organic coordination compounds, having potential applications due to their crystallinity, high porosity, designability and adjustability of structure and properties.[1–7] The development of proton conductors that answer to stimuli is of interest not only in terms of practical applications such as drug delivery, sensors, memory, and display devices, but also for gaining a better knowledge of proton transport pathways.[8,9] They typically operate at low temperatures (20–80 °C) with the aid of water. The two proton donor and two

acceptor sites on the oxygen atom enable water to create an H-bonding network with a tetrahedral shape, which is helpful for effective proton hopping through local molecule rotational motions. Water also forms a degenerate conjugate acid–base system. Moreover, the utilization of a neutral liquid phase facilitates the manipulation process, while its diminutive molecular size enables dynamic molecular motion during diffusion and mobility.[5,6]

It is well known that proton transport occurs through proton hopping over a network of hydrogen bonds (H-bonds). As a result, it has been extensively studied how to build this network for efficient proton transport, which is a key investigative aspect of proton conductors. Coordination compounds have been shown to be interesting systems for the modelling of H-bonding networks due to the wide range of possible configurations.[1–6] Unfortunately, it is challenging to show that the structural alteration of the proton conduction pathway and the proton conductivity are related.[1–4]

The simplest method to introduce proton carriers is to embed a counterion such as hydronium (H_3O^+), ammonium [NH_4^+, $(CH_3)_2NH_2^+$,...] or an anion (SO_4^{2-}), forming the charged compounds. The counterions create proton

Ruđer Bošković Institute, Bijenička cesta 54, 10000 Zagreb, Croatia.
E-mail: Marijana.Juric@irb.hr

conducting channels by forming H-bonding arrays with the guest water or other chemical ingredients. The addition of functionalized structural elements, such as noncoordinated functional groups in organic ligands (such as –OH, –NH$_2$, –COOH, –SO$_3$H, and –PO$_3$H$_2$), or the coordination of a metal centre with useful molecules like H$_2$O, EtOH, and imidazole can also result in conductivity.[1–6]

Because of its many options for coordination to metal centres and its capacity to mediate electrical effects between paramagnetic metal ions, the oxalate moiety, C$_2$O$_4^{2-}$, plays a crucial role in the design and synthesis of multifunctional materials.[10–13] In recent years, research on homo- and heterometallic oxalate-based compounds has focused heavily on both their magnetic and proton conducting properties.[14–29] Due to the impact of humidity and temperature, proton conductive materials must have strong water and chemical durability. In general, oxalate-based systems have regular structures and sturdy frameworks. Additionally, the oxalate group's oxygen atoms can build intricate hydrogen-bonded networks with water that are ideal for proton conduction. Although two-dimensional (2D) and three-dimensional (3D) oxalate-based assemblies frequently exhibit high proton conductivity,[14–28,30,31] low-dimensional structures can also exhibit excellent proton conductivity properties *via* the H-bonding chain because a small void space can be beneficial for proton hopping.[4] In our earlier research, we described a one-dimensional (1D) oxalate-bridged coordination polymer of iron(III), {[NH(CH$_3$)(C$_2$H$_5$)][FeCl$_2$(C$_2$O$_4$)]}$_n$, with H-bonded cationic diethylmethylammonium moieties, which results in extremely high room-temperature proton conductivity and exceptional humidity-sensing properties [2.70 × 10^{-4} (Ω cm)$^{-1}$ under 93% relative humidity (RH) conditions].[29] Motivated by this result, we have investigated the proton conduction behaviour of the new oxalate-based compounds of iron(III) obtained with different ammonium components: mononuclear (NH$_4$)$_2$[Fe(H$_2$O)Cl$_3$(C$_2$O$_4$)]·H$_2$O (1), as well as 1D {[NH(CH$_3$)$_2$(C$_2$H$_5$)][FeCl$_2$(C$_2$O$_4$)]·H$_2$O}$_n$ (2) and {[N(CH$_3$)(C$_2$H$_5$)$_3$][FeCl$_2$(C$_2$O$_4$)]}$_n$ (3).

This paper presents an analysis of the proton conductivity of compounds 1–3 at room temperature (RT). Of particular interest is compound 1, which forms a three-dimensional hydrogen-bonded network. The conductivity of compound 1 exhibits a significant increase of nearly seven orders of magnitude as the RH value increases. At 25 °C and 74% relative humidity, the conductivity reaches a remarkably high value of 2.17 × 10^{-3} (Ω cm)$^{-1}$. The investigation of the conductivity of discrete mononuclear structures, which have a tendency to build a supramolecular framework through weak contacts including stacking interactions and complex hydrogen bonding networks, is a topic that has received limited attention and lacks substantial research.[32]

In conjunction with impedance spectroscopy, the compounds acquired were subjected to characterization using powder and single crystal X-ray diffraction, as well as IR spectroscopy.

Results and discussion

Synthesis and crystal structure of compounds 1–3

The yellow polyhedral crystals of compound {[NH(CH$_3$)$_2$(C$_2$H$_5$)][FeCl$_2$(C$_2$O$_4$)]·H$_2$O}$_n$ (2) were prepared by slow evaporation of an aqueous solution containing a mixture of FeCl$_3$, H$_2$C$_2$O$_4$·2H$_2$O and dimethylethylamine (C$_2$H$_5$)(CH$_3$)$_2$N. Furthermore, yellow crystals of compounds (NH$_4$)$_2$[Fe(H$_2$O)Cl$_3$(C$_2$O$_4$)]·H$_2$O (1) and {[N(CH$_3$)(C$_2$H$_5$)$_3$][FeCl$_2$(C$_2$O$_4$)]}$_n$ (3) were prepared similarly, except that the cations NH$_4^+$ and (C$_2$H$_5$)$_3$(CH$_3$)N$^+$, respectively, were added directly to the reaction mixture. Interestingly, the known 3D coordination polymer {(NH$_4$)$_2$[Fe$_2$O(C$_2$O$_4$)$_2$Cl$_2$]·2H$_2$O}$_n$ crystallizes when ammonia is used for the synthesis instead of the salt NH$_4$Cl.[33]

The crystal structure of the oxalate compound (NH$_4$)$_2$[Fe(H$_2$O)Cl$_3$(C$_2$O$_4$)]·H$_2$O (1), crystallizing in the monoclinic space group $P2_1/m$, consists of two ammonium cations NH$_4^+$, a mononuclear anion [Fe(H$_2$O)Cl$_3$(C$_2$O$_4$)]$^{2-}$, and a crystal water molecule. The mirror planes pass through the iron(III) ion, the coordinated water molecule, a chloride ion, the C–C bond of the oxalate group, as well as the nitrogen atoms of both ammonium cations, and the oxygen atom of the water of crystallization (Fig. 1 and S1†). The Fe atoms display an octahedral FeO$_3$Cl$_3$ coordination involving two O atoms of the bidentate oxalate group and two Cl atoms in the equatorial plane, together with a third chloride atom (Cl2) and water molecules (O3) in the apical positions. Selected bond distances and angles are summarized in Table S1.† The values of the Fe–Cl and Fe–O bond lengths in 1 are slightly longer than those found for the corresponding bonds in the similar mononuclear iron(III) compound (C$_6$H$_{14}$N$_2$)[Fe(C$_2$O$_4$)Cl$_2$(H$_2$O)$_2$]Cl.[34]

The oxygen atoms of the oxalate group, chloride ions, coordinated and crystal water molecules and NH$_4^+$ cations construct an abundant hydrogen bonding network; a total of 11 symmetry-independent hydrogen bonds (Table S2†) connect anions, cations, and water molecules into a 3D arrangement (Fig. 2).
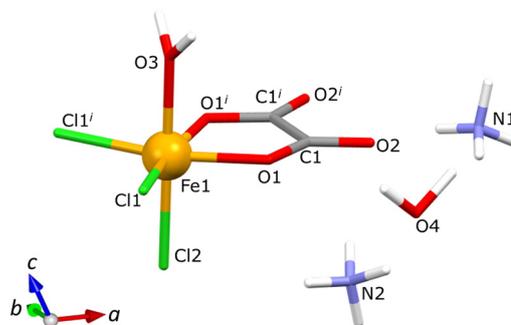

Fig. 1 Molecular structure of the mononuclear compound (NH$_4$)$_2$[Fe(H$_2$O)Cl$_3$(C$_2$O$_4$)]·H$_2$O (1). Symmetry operator: (*i*) *x*, 1/2 − *y*, *z*.
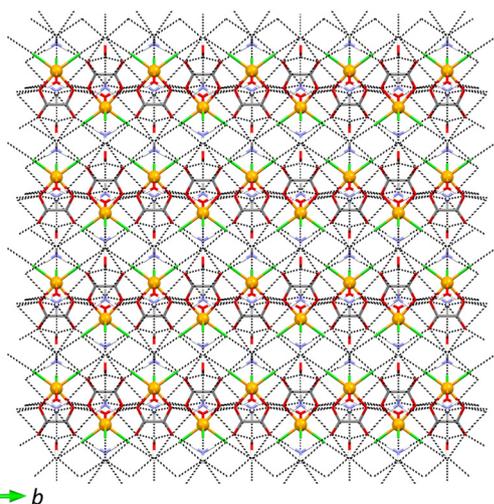
Fig. 2 A 3D hydrogen-bonding network in the crystal packing of compound $(NH_4)_2[Fe(H_2O)Cl_3(C_2O_4)]\cdot H_2O$ (**1**) viewed in the direction [100].

The structure of compound $\{[NH(CH_3)_2(C_2H_5)][FeCl_2(C_2O_4)]\cdot H_2O\}_n$ (**2**) consists of infinite anionic zig-zag chains $[FeCl_2(C_2O_4)]_n^{n-}$ with the iron(III) ions linked by bis(bidentate) oxalate groups, dimethylethylammonium cations $(C_2H_5)(CH_3)_2NH^+$, and crystal water molecules (Fig. 3 and S2†). Each metal centre is coordinated by two oxalate ligands in a *cis* arrangement and two terminal Cl^- ions. The values of the Fe–O and Fe–Cl bond lengths agree well with those of similar 1D coordination polymers of iron(III) ions containing alkylammonium cations (Table S1†).[29,35–39]

The $Fe1\cdots Fe1^i$ and $Fe1\cdots Fe1^{ii}$ [symmetry operators: (i) $-x$, $-y$, $2-z$; (ii) $-x$, $1-y$, $2-z$] distances across the bridging oxalate group are 5.4863(11) Å and 5.5063(11) Å, respectively.

Compared to a similar compound $\{[NH(CH_3)(C_2H_5)_2][FeCl_2(C_2O_4)]\}_n$, which exhibits two reversible phase transitions: from the high-temperature phase to the mid-temperature phase

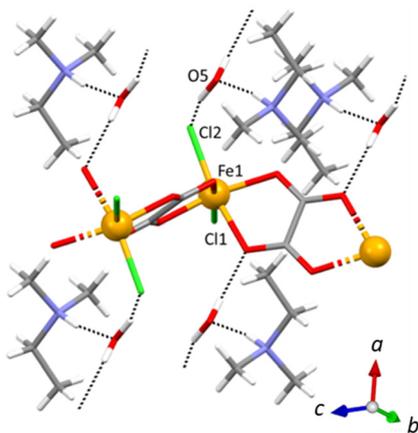at $T \sim 213$ K and from the mid-temperature phase to the low-temperature phase at $T \sim 120$ K,[29] the determination of the unit cell of **2** at RT and 100 K indicates that there is no phase transition. Namely, it crystallizes with one water molecule because there is one less methylene group in the used amine, and probably there is no temperature-induced structural flexibility due to the existence of water and the corresponding hydrogen bonds (Fig. 3 and 4).

In addition, compound $\{[N(CH_3)(C_2H_5)_3][FeCl_2(C_2O_4)]\}_n$ (**3**), crystallizing in the space group $P2_1/n$, contains the already known and mentioned infinite anionic zig-zag chains $[FeCl_2(C_2O_4)]_n^{n-}$ as compound **2** (ref. 29 and 35–39) and triethylmethylammonium cations $(C_2H_5)_3(CH_3)N^+$ (Fig. 5a and S3†). A detailed analysis of its geometry is not straightforward due to the disorder (see the Experimental

(a)

(b)

(c)
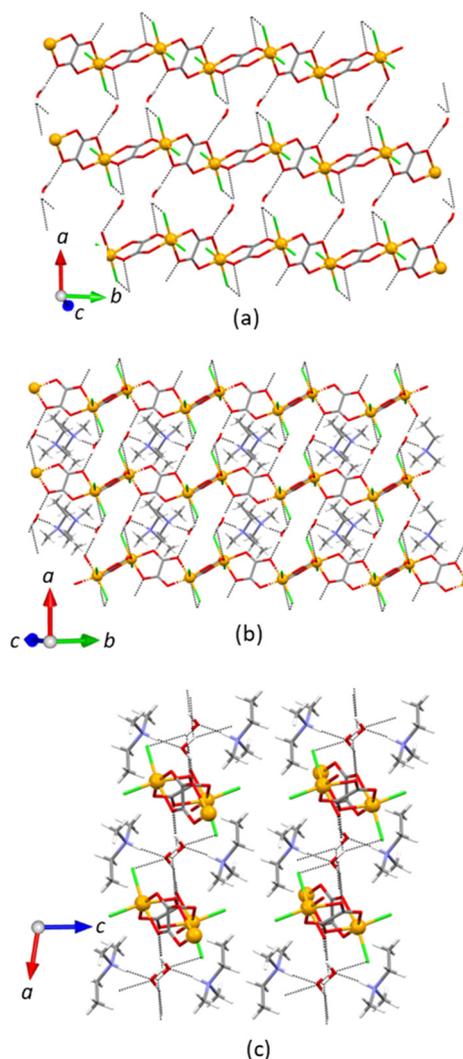
Fig. 4 The 2D hydrogen-bonding pattern in the (100) plane (a) in the crystal packing of $[FeCl_2(C_2O_4)]_n^{n-}$ and water molecules and (b) with hydrogen-bonded $(C_2H_5)(CH_3)_2NH^+$ cations; (c) crystal packing of coordination polymer $\{[NH(CH_3)_2(C_2H_5)][FeCl_2(C_2O_4)]\cdot H_2O\}_n$ (**2**) viewed in the [010] direction.

Fig. 3 A part of the $[FeCl_2(C_2O_4)]_n^{n-}$ chain with hydrogen-bonded crystal water molecules and cations $(C_2H_5)(CH_3)_2NH^+$ in coordination polymer **2**.
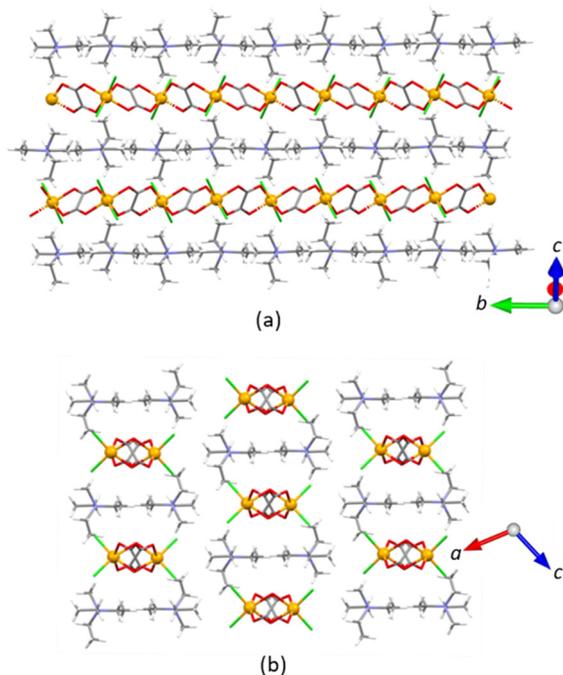
Fig. 5 Crystal packing of the cations $(C_2H_5)_3(CH_3)_2N^+$ and the anionic chains $[FeCl_2(C_2O_4)]_n^{n-}$ in coordination polymer **3**: (a) in the (100) plane and (b) viewed in the [010] direction.

section). However, geometric parameters describing the coordination sphere of the iron(III) at RT can be found in Table S1.† The distances between the iron(III) centres across the oxalate bridges correspond to the values in similar compounds.[29,35–39] There are no N–H···O or O–H···O hydrogen bonds between the infinite anion and cations, which was expected since the cation has no strong proton donors; only the hydrogen atoms of the methylene and ethylene groups are involved in the formation of weaker C–H···O hydrogen bonds.

Infrared study and thermal analysis of compounds 1–3

The IR spectra of the prepared complexes are in agreement with the results of the X-ray analysis: the presence of oxalate groups and alkyl- and/or ammonium cations (Fig. S4†). The bands located at $3270w–2640w$ cm^{-1} could be recognized as ν(C–H) and ν(N–H) due to the presence of alkylammonium cations in **2** and **3**, in addition to the bands present in the range $1447m–1484m$ cm^{-1} and $1100–950$ cm^{-1} ascribed to the C–N stretching. In the spectrum of **1**, the ammonium ion shows a strong broad NH_4^+ bending band near 1400 cm^{-1}. In general, the N–H bending band of the tertiary amine salts is weak.[40]

The infrared spectra confirmed the presence of the uncoordinated (bidentate mode in compound **1**) and coordinated [bis(bidentate) mode in compounds **2** and **3**] CO groups of the oxalate ligand. The absorption bands characteristic of oxalate ligands for all the compounds are summarized in Table S3.†[29,35]

The thermal behavior of the title compounds was studied by thermogravimetric (TG) analysis on the crystalline samples in a stream of synthetic air up to 1000 °C, and the corresponding curves are shown in Fig. S5.† Compounds undergo several successive decomposition processes, with the main mass loss corresponding to the release of the (alkyl) ammonium cations, the chloride ions and the oxalate group, with some closely and not distinctive steps in the TG curves. The decomposition of the simplest salt **1** starts with heating and ends around 470 °C. Compound **3** is stable up to 180 °C, and decomposition slows down around 600 °C, while the mass does not change on further heating to 1000 °C. For the similar compound **2**, the remaining mass stays constant after 725 °C, which can be explained by a stronger interaction between cations and anions.

Proton conductivity of compounds 1–3

The Nyquist plot for the samples measured in a dry nitrogen atmosphere at 30 °C is shown in Fig. 6. The spectra consist of a well-defined semicircle, corresponding to the conduction process through the bulk, and a small spur at low frequencies, possibly due to the blocking of protons on the surface of metallic electrodes. In order to obtain DC conductivity values for each sample, the spectra were modelled by a corresponding equivalent electrical circuit model consisting of a parallel combination of a resistor and a constant phase element (CPE 1), representing the bulk response, and an additional constant phase element (CPE 2), representing the spur.

The studied compounds were found to be extremely sensitive to humidity conditions (Table S4†), especially **1**, for which the σ_{DC} increased by almost seven orders of magnitude, from 4.59×10^{-11} $(\Omega$ cm$)^{-1}$ at 10% RH to very high 2.17×10^{-3} $(\Omega$ cm$)^{-1}$ at 74% RH (Fig. 7a). However, after the rapid conductivity response to the changes in relative

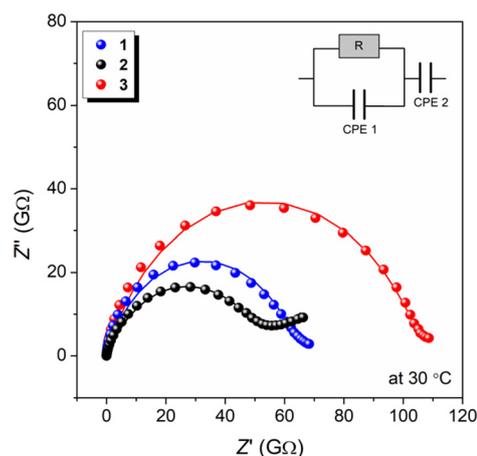**Fig. 6** Nyquist plot for compounds **1–3** measured in a dry nitrogen atmosphere at 30 °C (experimental data are shown as circles and model fitting curves as solid lines). The inset shows an Arrhenius-type plot of the DC conductivity for studied samples.
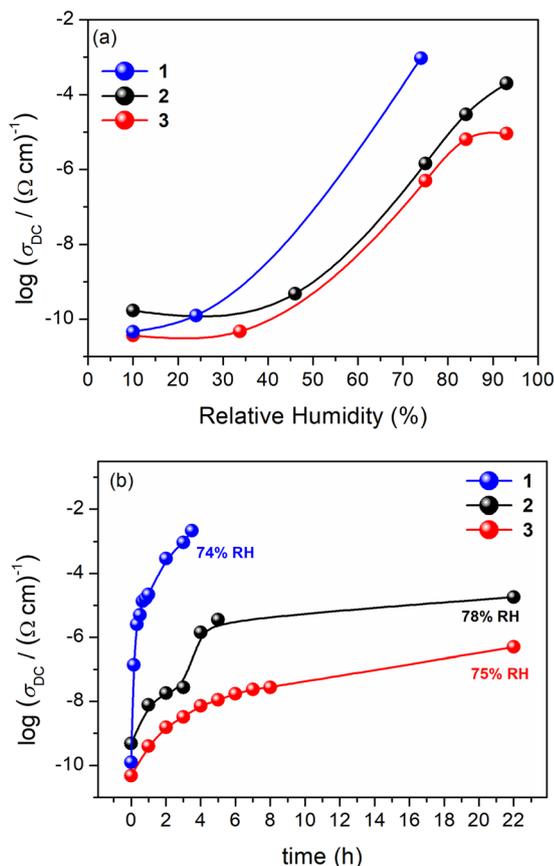
Fig. 7 (a) The proton conductivity as a function of relative humidity (RH) at room temperature for compounds **1–3**; (b) time-dependent conductivity tests for compounds **1–3** at ≈75% RH.

humidity, the sample becomes deliquescent after 4 hours of measurement, preventing further measurements above the maximum allowable humidity (Fig. 7b). On the other hand, in the range from 10% to 93% RH compounds **2** and **3** showed an increase in conductivity of six and five orders of magnitude reaching values of 2.00×10^{-4} $(\Omega \text{ cm})^{-1}$ and 9.17×10^{-6} $(\Omega \text{ cm})^{-1}$, respectively, both at 25 °C and 93% RH (Fig. 7a). In contrast to **1**, these compounds were able to maintain stable proton conductivity over a period of 18 h at ~75% relative humidity (Fig. 7b). Similar time-dependent tests were performed with samples **2** and **3** at RH = 84% and 93%, which showed the same behaviour and confirmed the good stability under high humid conditions.

No change in the structures of **1–3** was observed after treatment with humidity; the good overlap of the powder X-ray diffraction (PXRD) patterns of as-synthesized and humidity-treated samples confirms the water stability of the studied compounds (Fig. S6–S8†).[25,28,41] In order to explore compounds as promising candidates for the development of solid-state electrolytes or as switchable materials, their structural integrity must be ensured so that they retain their original functionalities and properties under operating conditions. Therefore, water stability is always a prerequisite for studying the proton conductivity of coordination

compounds under humid conditions.[6] One of the reasons why **1** exhibits deliquescent behavior at lower relative humidity may be related to its more unstable structure, consisting of mononuclear anions $[Fe(H_2O)Cl_3(C_2O_4)]^{2-}$ linked only by relatively weak hydrogen bonds to water molecules and ammonium cations (the D···A distances are in the range 2.752(13)–3.469(9) Å, Table S2†), in contrast to the polymeric chain of iron(III) ions, $[FeCl_2(C_2O_4)]_n^{n-}$, bridged by bis(bidentate)oxalate ligand in compounds **2** and **3**.

The mononuclear compound **1** has the highest proton conductivity compared to 1D compounds **2** and **3**. The existence of a total of 11 symmetry-independent hydrogen bonds between the oxalate group and the chloride ions of the anions $[Fe(H_2O)Cl_3(C_2O_4)]^{2-}$, the cations NH_4^+ and the water molecules (one coordinated and one crystalline) forms a 3D hydrogen bonding network which acts as a pathway that allows the fastest diffusion process and high proton conductivity (Fig. 2, Table S2†).[32,42–44] In fact, NH_4^+ ions as proton carriers play an essential role in the construction of efficient H-bond networks. This direct relationship between the drastic increase in proton conductivity and the increase in humidity confirms that proton transport action in **1** is associated with water adsorption.[42] It is presumed that the adsorbed water molecules help the diffusion of protons and serve as mediators through the formed hydrogen bond network, which is responsible for such high conduction with increasing RH.[43]

A similarly high value for proton conductivity of 1.3×10^{-3} $(\Omega \text{ cm})^{-1}$ at 98% RH, compared with 2.17×10^{-3} $(\Omega \text{ cm})^{-1}$ of **1**, was found for the 1D ferro-oxalate polymer compound $[Fe(H_2O)_2(C_2O_4)]_n$ which contained two coordinated water molecules that formed a 1D ordered array suitable for fast proton transport.[45] Most importantly, the value of conductivity of **1** is slightly lower than that $[1.16 \times 10^{-3}$ $(\Omega \text{ cm})^{-1}]$ of the first mononuclear proton conductive compound published recently, namely $[Dy(H_2bim)_2(H_2O)_2(NO_3)_2](NO_3)$ (H_2bim = 2,2′-biimidazole) obtained at 100% RH and 35 °C. Crystal structure analysis shows that the H_2bim molecules form strong and rich hydrogen bonding interactions with the coordinated water molecules and nitrate groups to form a 1D H-bonding network, which play a dominant role in the high conductivity of this mononuclear compound.[32] This confirms that the density of the formed H-bonds in **1** is one of the key factors for the mobility of protons, and it is beneficial for its high conductivity. Namely, the density of active protons positively impacts the proton conducting property in nonporous structures.[32,43,44] This maximum proton conductivity value of **1** is also comparable to other highly proton conductive 2D and 3D oxalate-bridged coordination polymers containing also NH_4^+ cations: 3D $\{(NH_4)_4[MnCr_2(C_2O_4)_6]\cdot 4H_2O\}_n$ $[1.1 \times 10^{-3}$ $(\Omega \text{ cm})^{-1}$, 96% RH],[14] 3D $\{(NH_4)_5[Mn_2Cr_3(C_2O_4)_9]\cdot 10H_2O\}_n$ $[7.1 \times 10^{-4}$ $(\Omega \text{ cm})^{-1}$, 74% RH][15] or 2D $\{(NH_4)_2(adp)[Zn_2(C_2O_4)_3]\cdot 3H_2O\}_n$ [adp = adipic acid; 8×10^{-3} $(\Omega \text{ cm})^{-1}$, 98% RH][20] and $\{(NH_4)_2(H_2adp)[Zn_2(C_2O_4)_3]\cdot 2H_2O\}_n$ $[\sim 7 \times 10^{-5}$ $(\Omega \text{ cm})^{-1}$, 95% RH].[21]

Compound $\{[NH(CH_3)_2(C_2H_5)][FeCl_2(C_2O_4)]\cdot H_2O\}_n$ (**2**) and the previously reported $\{[NH(CH_3)(C_2H_5)_2][FeCl_2(C_2O_4)]\}_n$ (ref.

29) have the same anionic chain, although they are not isostructural, and show nearly identical proton conductivity behaviour as a function of relative humidity (Table S4†); the lack of one methylene group and the presence of one crystalline water molecule in **2** have no significant effect on the proton conductivity and, moreover, prevent the phase transition due to the existence of additional hydrogen bonds.

It is known that the hydrophilicity of cationic R_3NH^+ ions decreases with increasing bulkiness of the residue, which is closely related to the affinity for water molecules.[16,24] Thus, the dimethylethylammonium cation has higher hydrophilicity compared to the triethylmethylammonium cation in $\{[N(CH_3)(C_2H_5)_3][FeCl_2(C_2O_4)]\}_n$ (**3**), free of N–H···O or O–H···O hydrogen bonds between the anion and the cations, which in combination with the protonation results in relatively high conductivity in **2**. A strong conductivity enhancement of **2** and **3** with the increase in relative humidity (Fig. 7a, Table S4†) suggests that in these compounds the association of water molecules does not only work as media to tune the concentration of protons but also participates in the construction of the efficient conducting pathways for protons through the formation of a continuous hydrogen-bond network.[1,20]

Conclusions

In summary, three novel oxalate-based compounds of iron(III) containing different (alkyl)ammonium cations were prepared, and their proton conductivity was investigated: $(NH_4)_2[Fe(H_2O)Cl_3(C_2O_4)]\cdot H_2O$ (**1**), $\{[NH(CH_3)_2(C_2H_5)][FeCl_2(C_2O_4)]\cdot H_2O\}_n$ (**2**) and $\{[N(CH_3)(C_2H_5)_3][FeCl_2(C_2O_4)]\}_n$ (**3**). Comparing their structures and values of proton conductivity it can be concluded and confirmed that the amount of protonated proton carriers acting as proton donors, the number of non-protonated sites acting as proton acceptors, and the efficient proton transport pathway made of the H-bonding network are extremely important for obtaining materials with high conductivity, rather than their dimensional arrangement.[32,44] Mononuclear compound **1** has a very high conductive property derived from a 3D H-bonding network that serves as an effective proton transfer path formed by the excellent proton carriers NH_4^+ ions together with water molecules, and the bidentate coordinated oxalate group and chloride anions as H-bonding acceptors. Coordination polymer **2**, containing $(CH_3)_2(C_2H_5)NH^+$ cations, has a lower amount of proton donors, which also reduces the density of hydrogen bonds and consequently leads to weaker conductive pathways for protons. As expected, compound **3** has the lowest conductivity because it does not contain protonated proton carriers and has a lower affinity for water.

Since the studied compounds exhibit an increase in conductivity more than six orders of magnitude with increasing RH, they suggest potential switching behaviour stimulated by guest molecules; therefore they have the potential to be further investigated as conductivity-switching

devices in response to external stimuli of atmospheric composition.[9]

Based on the achieved results, our further research would be related to the electrical characterization of (novel) discrete mononuclear oxalate complexes containing suitable proton carriers, which have not yet been investigated in detail for proton transport.

Experimental

Materials and physical measurements

The chemicals utilized in the study were obtained from commercial suppliers and were employed without undergoing additional purification processes. The infrared spectra were obtained by employing KBr pellets as a medium and utilizing a Bruker Alpha-T spectrometer within the range of 4000–350 cm^{-1}. Thermal analysis of compounds **1**–**3** was performed on a Netzsch STA 449 F5 Jupiter thermal analyzer, in the range from RT to 1000 °C, in a stream of synthetic air, at a heating rate of 10 °C min^{-1}.

Synthetic procedures

Synthesis of $(NH_4)_2[Fe(H_2O)Cl_3(C_2O_4)]\cdot H_2O$ (1). An aqueous solution (2 mL) of NH_4Cl (0.1072 g; 0.2 mmol) was added to the mixed aqueous solutions of $FeCl_3$ (5 mL; 0.1622 g; 1 mmol) and $H_2C_2O_4\cdot 2H_2O$ (5 mL; 0.1261 g; 1 mmol). After the yellow solution slowly evaporated, prismatic single crystals of **1** appeared within two weeks. The isolated crystals were promptly rinsed with a small quantity of ethanol and afterwards air-dried. The yield was 35%. IR data (KBr, cm^{-1}): 3494 (s), 3250 (s), 3027 (s), 2812 (m), 2344, 1709 (s), 1673 (vs), 1397, 1262, 905 (m), 794 (m), 594 (w), 537 (w), 481 (w).

Synthesis of $\{[NH(CH_3)_2(C_2H_5)][FeCl_2(C_2O_4)]\cdot H_2O\}_n$ (2). N,N-Dimethylethylamine, $N(CH_3)_2(C_2H_5)$, (2.2 mmol; 0.227 mL) was mixed with an aqueous solution (10 mL) which contains $FeCl_3$ (0.1622 g; 1 mmol) and $H_2C_2O_4\cdot 2H_2O$ (0.1261 g; 1 mmol). After two weeks of slow evaporation of the clear solution, yellow rod-like single crystals of **2** formed. They were promptly rinsed by a small amount of ethanol and afterwards air-dried. The obtained yield was 40%. IR data (KBr, cm^{-1}): 3564 (m), 3465 (m), 3132 (w), 3054 (w), 2955 (sh), 2924 (m), 2854 (w), 2750 (w), 2528 (sh), 1694 (vs), 1609 (vs), 1469 (m), 1440 (w), 1414 (w), 1395 (w), 1384 (w), 1350 (m), 1307 (m), 1188 (w), 1084 (w), 1070 (w), 1061 (w), 993 (w), 924 (w), 805 (m), 474 (w), 450 (w), 425 (w).

Synthesis of $\{[N(CH_3)(C_2H_5)_3][FeCl_2(C_2O_4)]\}_n$ (3). To an aqueous solution (10 mL) containing $FeCl_3$ (0.1622 g; 1 mmol) and $H_2C_2O_4\cdot 2H_2O$ (0.1261 g; 1 mmol), the aqueous solution (2 mL) of N,N-triethylmethylamine, $N(CH_3)(C_2H_5)_3$ (0.1518 g; 2 mmol) was added. The reaction mixture was stirred for 10 min. After almost all the solution had evaporated, yellow rod-like single crystals of **3**, together with light orange crystallites (indicated as ionic oxalate salt by IR spectroscopy) began to form. Mechanically separated crystals were quickly washed with a small amount of ethanol and dried in air. The yield was 37%. IR data (KBr, cm^{-1}): 3368 (m,

br), 2989 (w), 292 (w), 1697 (s),1609 (vs), 1494, 1459, 1448, 1397, 1350 (m), 1307 (m), 1219 (w), 1192 (w), 1125 (w), 1077 (w), 1048 (w), 1004 (w), 964 (w), 808 (m), 535 (w), 492 (w), 475 (w), 452(w), 422 (w).

Single-crystal X-ray structural study

The X-ray data for single crystals of compounds **1** and **2** were collected by ω-scans on an Oxford Diffraction Xcalibur Nova R diffractometer with mirror-monochromated Cu-Kα radiation (λ = 1.54179 Å, microfocus tube, CCD detector) at 293(2) K (**1**) and 100 K (**2**). Crystal of **3** were measured on an Oxford Diffraction Synergy S diffractometer equipped with an Oxford Cryosystems Cryostream Series 800 cooling device, using Cu-Kα radiation (λ = 1.54179 Å, microfocus tube, pixel detector). Data reduction, including the multi-scan absorption correction, was performed by using the CrysAlisPRO[46] software package. The structures were solved using SHELXS97 (ref. 47) and refined with SHELXL-2017/1 within the WinGX software package.[48] The full-matrix least squares refinement was used to refine the models; all non-hydrogen atoms were refined anisotropically. Hydrogen atoms bound to C atoms were modelled as riding entities, while hydrogen atoms of water molecules were located in difference Fourier maps and refined with O–H bond length

restrained to 0.95(2) Å and HOH angles were restrained by restraining the intramolecular H⋯H distance to 1.50(4) Å. Compound **3** at room temperature yielded a rather poor, albeit undisordered, structure, with unacceptably high R values and residual density exceeding 1.8 e Å^{-3}. However, at 100 K the structure was badly disordered. Since attempts to refine the structure in a lower symmetry or a larger unit cell always yielded disorder, we conclude that the nature of this disorder is statistic, rather than a presence of a supercell. In the iron-oxalate chains two positions of chloride and oxalate ligands are present, with respective occupancies of 0.90 and 0.10. The cations are also disordered over two positions, and their occupancies are 0.51 and 0.49, respectively. Thus, the molecular geometries at 100 K are not reliable, so we analysed only the RT structure. Geometrical calculations were carried out using PLATON[49] and the figures were made by the use of the CCDC-Mercury[50] and VESTA programs.[51] Crystallographic and refinement data for the structures reported in this paper are shown in Table 1.

Powder X-ray structural study

The powder X-ray diffraction data (PXRD) at room temperature for compounds **1**–**3** was collected on a Malvern Panalytical Empyrean diffractometer using a step size of 0.001° in the 2

Table 1 Crystallographic data and structure refinement details for compounds $(NH_4)_2[Fe(H_2O)Cl_3(C_2O_4)]\cdot H_2O$ (**1**), $\{[NH(CH_3)_2(C_2H_5)][FeCl_2(C_2O_4)]\cdot H_2O\}_n$ (**2**) and $\{[N(CH_3)(C_2H_5)_3][FeCl_2(C_2O_4)]\}_n$ (**3**)

Compounds	1	2	3-RT	3–100 K
Empirical formula	$C_2H_{12}Cl_3FeN_2O_6$	$C_6H_{14}Cl_2FeNO_5$	$C_9H_{18}Cl_2FeNO_4$	$C_9H_{18}Cl_2FeNO_4$
Formula wt/g mol^{-1}	322.34	306.93	330.99	330.99
Colour	Yellow	Yellow	Yellow	Yellow
Crystal dimensions/mm	0.19 × 0.13 × 0.10	0.43 × 0.15 × 0.12	0.08 × 0.07 × 0.02	0.08 × 0.07 × 0.02
Space group	$P2_1/m$	P-1	$P2_1/n$	$P2_1/n$
a/Å	9.0027(3)	7.4880(3)	11.2283(16)	11.2146(5)
b/Å	7.5270(2)	8.5970(4)	8.6109(9)	8.5542(3)
c/Å	9.0306(4)	9.8960(3)	16.306(3)	15.9856(7)
α/°	90	90.603(3)	90	90
β/°	114.109(5)	99.679(3)	109.460(19)	109.469(4)
γ/°	90	95.105(3)	90	90
Z	2	2	4	2
V/Å^3	558.56(4)	625.28(4)	1486.5(4)	1445.84(11)
D_{calc}/g cm^{-3}	1.917	1.630	1.479	1.520
μ/mm^{-1}	17.573	13.665	11.488	11.810
λ/Å	1.54179 (CuKα)	1.54179 (CuKα)	1.54179 (CuKα)	1.54179 (CuKα)
$F(000)$	326	314	684	684
θ range/°	5.37–75.79	5.167–76.308	4.21–67.68	4.23–67.86
T/K	293(2)	100(2)	293(2)	100(2)
Range of h, k, l	−11 < h < 11	−9 < h < 9	−9 < h < 13	−14 < h < 10
	−6 < k < 9	−8 < k < 10	−10 < k < 10	−10 < k < 10
	−11 < l < 11	−12 < l < 12	−20 < l < 20	−17 < l < 20
Reflections collected	3912	8586	18 962	10 979
Independent reflections	1249	2503	3167	3063
Observed reflections ($I \geq 2\sigma$)	1154	2302	1459	2581
R_{int}	0.0848	0.0784	0.2874	0.0506
R, wR [$I \geq 2\sigma$]	0.0790; 0.2251	0.0621, 0.2126	0.1530, 0.4212	0.0733; 0.1934
Goodness-of-fit	1.149	1.447	1.212	1.021
H atom treatment	Mixed	Mixed	Riding	Riding
No. of parameters, restraints	92, 17	142, 3	154, 61	219, 44
$\Delta\rho_{max}$, $\Delta\rho_{min}$, $\Delta\rho_{rms}$ (e Å^{-3})	1.665, −1.115, 0.214	1.227, −1.003, 0.186	1.837, −0.596, 0.242	0.913, −0.749, 0.121

theta region between 5° and 50°. Program HighScoreXpert Plus (Version 4.5, March 2016) was used for comparison of the experimental and theoretical data.

Electrical study

The electrical conductivity of samples **1**–**3** was measured by impedance spectroscopy (Novocontrol Alpha-AN dielectric analyzer) in a frequency range from 0.01 Hz to 1 MHz at different temperature and humidity conditions. Pellets of the polycrystalline samples of a thickness: 0.33, 0.93 and 0.44 mm for **1**, **2** and **3** respectively, were first prepared after which gold electrodes (3.8 mm in diameter) were sputtered on opposite surfaces of the samples. For temperature-dependent measurements, a sample was placed in a cell with dry nitrogen and measured isothermally at temperatures from −50 °C to 30 °C with a temperature step of 10 °C. Measurements were conducted at room temperature to investigate the influence of humidity. The relative humidities considered were: ambient conditions, 75%, 84%, and 93%. The measurement of relative humidity within the sample cell was conducted by utilizing saturated aqueous solutions containing various salts: NaCl (RH ∼ 75%), KCl (RH ∼ 84%) and KNO_3 (RH ∼ 93%). The impedance spectra were analysed by equivalent circuit modelling using the complex nonlinear least-squares fitting procedure (ZView software) while the DC conductivity was calculated from the values of electrical resistance (R) and electrode dimensions (A is the electrode area and d is the sample thickness) according to the equation: $\sigma_{DC} = d/(A \times R)$. The confirmation of phase purity in the bulk samples was achieved by comparing the PXRD pattern of compounds **1**–**3** with the PXRD pattern generated from their single-crystal analysis (Fig. S6–S8†).

Conflicts of interest

There are no conflicts to declare.

Acknowledgements

Notes and references

1 D.-W. Lim and H. Kitagawa, Proton transport in metal–organic frameworks, *Chem. Rev.*, 2020, **120**, 8416–8467.

2 Y. Ye, L. Gong, S. Xiang, Z. Zhang and B. Chen, Metal–Organic Frameworks as a Versatile Platform for Proton Conductors, *Adv. Mater.*, 2020, **32**, 1907090.

3 J. Su, W. He, X.-M. Li, L. Sun, H.-Y. Wang, Y.-Q. Lan, M. Ding and J.-L. Zuo, High Electrical Conductivity in a 2D MOF with Intrinsic Superprotonic Conduction and Interfacial Pseudo-capacitance, *Matter*, 2020, **2**, 711–722.

4 X.-X. Xie, Y.-C. Yang, B.-H. Dou, Z.-F. Li and G. Li, Proton conductive carboxylate-based metal-organic frameworks, *Coord. Chem. Rev.*, 2020, **403**, 213100.

5 D.-W. Lim and H. Kitagaw, Rational strategies for proton-conductive metal–organic frameworks, *Chem. Soc. Rev.*, 2021, **50**, 6349–6368.

6 D.-W. Lim, M. Sadakiyo and H. Kitagawa, Proton transfer in hydrogen-bonded degenerate systems of water and ammonia in metal–organic frameworks, *Chem. Sci.*, 2019, **10**, 16–33.

7 K. Biradha, A. Goswami, R. Moi and S. Saha, Metal–organic frameworks as proton conductors: strategies for improved proton conductivity, *Dalton Trans.*, 2021, **50**, 10655–10673.

8 F. Bigdeli, C. T. Lollar, A. Morsali and H. C. Zhou, Switching in Metal-Organic Frameworks, *Angew. Chem., Int. Ed.*, 2020, **59**, 4652–4669.

9 F. Xiang, S. Chen, Z. Yuan, L. Li, Z. Fan, Z. Yao, C. Liu, S. Xiang and Z. Zhang, Switched Proton Conduction in Metal-Organic Frameworks, *JACS Au*, 2022, **2**, 1043–1053.

10 L. Kanižaj, L. Androš Dubraja, F. Torić, D. Pajić, K. Molčanov, E. Wenger and M. Jurić, Dimensionality controlled by light exposure: 1D versus 3D oxalate-bridged [CuFe] coordination polymers based on an $[Fe(C_2O_4)_3]^{3-}$ metallotecton, *Inorg. Chem. Front.*, 2019, **6**, 3327–3335.

11 L. Kanižaj, D. Barišić, F. Torić, D. Pajić, K. Molčanov, A. Šantić, I. Lončarić and M. Jurić, Structural, Electrical, and Magnetic Versatility of the Oxalate-Based [CuFe] Compounds Containing 2,2′:6′,2″-Terpyridine: Anion Directed Synthesis, *Inorg. Chem.*, 2020, **59**, 18078–18089.

12 L. Molčanov, P. Šenjug, D. Barišić, D. Pajić, K. Molčanov and M. Jurić, Oxalate-based $[Cu^{II}Cr^{III}]$ coordination compounds affected by the tridentate ligand, simple anion, and reactant ratio: structural and magnetic features, *Dalton Trans.*, 2022, **51**, 16292–16306.

13 L. Kanižaj, K. Molčanov, F. Torić, D. Pajić, I. Lončarić, A. Šantić and M. Jurić, Ladder-like [CrCu] coordination polymers containing unique bridging modes of $[Cr(C_2O_4)_3]^{3-}$ and $Cr_2O_7^{2-}$, *Dalton Trans.*, 2019, **48**, 7891–7898.

14 E. Pardo, C. Train, G. Gontard, K. Boubekeur, O. Fabelo, H. Liu, B. Dkhil, F. Lloret, K. Nakagawa, H. Tokoro, S.-I. Ohkoshi and M. Verdaguer, High Proton Conduction in a Chiral Ferromagnetic MetalOrganic Quartz-like Framework, *J. Am. Chem. Soc.*, 2011, **133**, 15328–15331.

15 C. Maxim, S. Ferlay, H. Tokoro, S.-I. Ohkoshi and C. Train, Atypical stoichiometry for a 3D bimetallic oxalate-based long-range ordered magnet exhibiting high proton conductivity, *Chem. Commun.*, 2014, **50**, 5629–5632.

16 M. Sadakiyo, H. Ōkawa, A. Shigematsu, M. Ohba, T. Yamada and H. Kitagawa, Promotion of Low-Humidity Proton Conduction by Controlling Hydrophilicity in Layered Metal-Organic Frameworks, *J. Am. Chem. Soc.*, 2012, **134**, 5472–5475.

17 M. Sadakiyo, T. Yamada and H. Kitagawa, Hydroxyl Group Recognition by Hydrogen-Bonding Donor and Acceptor Sites

Embedded in a Layered Metal–Organic Framework, *J. Am. Chem. Soc.*, 2011, **133**, 11050–11053.

18 H. Ōkawa, M. Sadakiyo, T. Yamada, M. Maesato, M. Ohba and H. Kitagawa, Proton-Conductive Magnetic Metal–Organic Frameworks, {$NR_3(CH_2COOH)$}[$M_a^{II}M_b^{III}(ox)_3$]: Effect of Carboxyl Residue upon Proton Conduction, *J. Am. Chem. Soc.*, 2013, **135**, 2256–2262.

19 H. Ōkawa, A. Shigematsu, M. Sadakiyo, T. Miyagawa, K. Yoneda, M. Ohba and H. Kitagawa, Oxalate-Bridged Bimetallic Complexes {$NH(prol)_3$}[$MCr(ox)_3$] (M = Mn^{II}, Fe^{II}, Co^{II}; $NH(prol)_3^+$ = Tri(3-hydroxypropyl)ammonium) Exhibiting Coexistent Ferromagnetism and Proton Conduction, *J. Am. Chem. Soc.*, 2009, **131**, 13516–13522.

20 M. Sadakiyo, T. Yamada and H. Kitagawa, Rational Designs for Highly Proton-Conductive Metal−Organic Frameworks, *J. Am. Chem. Soc.*, 2009, **131**, 9906–9907.

21 M. Sadakiyo, T. Yamada, K. Honda, H. Matsui and H. Kitagawa, Control of Crystalline Proton-Conducting Pathways by Water- Induced Transformations of Hydrogen-Bonding Networks in a Metal−Organic Framework, *J. Am. Chem. Soc.*, 2014, **136**, 7701–7707.

22 M. Sadakiyo, T. Yamada and H. Kitagawa, Proton conductivity control by ion substitution in highly proton-conductive metal–organic framework, *J. Am. Chem. Soc.*, 2014, **136**, 13166–13169.

23 M. Sadakiyo, T. Yamada and H. Kitagawa, A study on proton conduction in a layered metal–organic framework, $Rb_2(adp)$[$Zn_2(ox)_3$]·$3H_2O$ (adp = adipic acid, $ox^{2−}$ = oxalate), *Inorg. Chem. Commun.*, 2016, **72**, 138–140.

24 M. Mon, J. Vallejo, J. Pasán, O. Fabelo, C. Train, M. Verdaguer, S. Ohkoshi, H. Tokoro, K. Nakagawa and E. Pardo, A novel xalate-based three-dimensional coordination polymer showing magnetic ordering and high proton conductivity, *Dalton Trans.*, 2017, **46**, 15130–15137.

25 S. S. Nagarkar, S. M. Unni, A. Sharma, S. Kurungot and S. K. Ghosh, Two-in-one: inherent anhydrous and water-assisted high proton conduction in a 3D metal-organic framework, *Angew. Chem., Int. Ed.*, 2014, **53**, 2638–2642.

26 S. Tominaka, F. Coudert, T. D. Dao, T. Nagao and A. K. Cheetham, Insulator-to-Proton-Conductor Transition in a Dense Metal–Organic Framework, *J. Am. Chem. Soc.*, 2015, **137**, 6428–6431.

27 X. Wang, T. Qin, S.-S. Bao, Y.-C. Zhang, X. Shen, L.-M. Zheng and D. Zhu, Facile synthesis of a water stable 3D Eu-MOF showing high proton conductivity and its application as a sensitive luminescent sensor for Cu^{2+} ions, *J. Mater. Chem. A*, 2016, **4**, 16484–16489.

28 A. Lozančić, S. Renka, D. Barišić, S. Burazer, K. Molčanov, D. Pajić and M. Jurić, High Proton Conductivity of Magnetically Ordered 2D Oxalate-Bridged [$Mn^{II}Cr^{III}$] Coordination Polymers with Irregular Topology, *Inorg. Chem.*, 2023, **62**, 9418–9428.

29 S. Burazer, K. Molčano, A. Šantić, T. Klase, E. Wenger, D. Pajić, Z. Jagličić, J. Popović and M. Jurić, Humidity-Sensing Properties of an 1D Antiferromagnetic Oxalate-Bridged Coordination Polymer of Iron(III) and Its Temperature-Induced Structural Flexibility, *Materials*, 2021, **14**, 5543.

30 J. Zhang, Q. Lei, L. Luan, H. Zeng, G. Zou and Z. Lin, N-Methylimidazolium containing metal phosphate–oxalates: solvent-free synthesis, crystal structure, and proton conduction, *CrystEngComm*, 2022, **24**, 743–746.

31 L. Huang, H. Xu, Y. Zhao, L. Huang, J. Bi, H. Zeng, G. Zou, D. Gao and Z. Lin, Isonicotinic acid-templated metal phosphate–oxalates: solvent-free synthesis, luminescence, and proton conduction, *CrystEngComm*, 2021, **23**, 6855–6858.

32 S.-D. Zhu, L. Dong, J.-J. Hu, H.-R. Wen, Y.-B. Lu, W.-H. Deng, C.-M. Liu, S.-J. Liu, G. Xu and Z.-H. Fu, A Proton Conductor Showing an Indication of Singleion Magnet Based on a Mononuclear Dy(III) Complex, *J. Mater. Chem. C*, 2021, **9**, 481–488.

33 D. Armentano, G. De Munno, F. Lloret, A. V. Palii and M. Julve, Novel Chiral Three-Dimensional Iron(III) Compound Exhibiting Magnetic Ordering at Tc = 40 K, *Inorg. Chem.*, 2002, **41**, 2007–2013.

34 Y. Cai, 4-Diazoniabicyclo[2.2.2] octanediaquadichlorido(oxalato-κ2O,O') iron(III) chloride, *Acta Crystallogr., Sect. E: Struct. Rep. Online*, 2009, **65**, m877.

35 H.-B. Xu, Z.-M. Wang, T. Liu and S. Gao, Synthesis, Structure, and Magnetic Properties of (A)[$Fe^{III}(oxalate)Cl_2$] (A = Alkyl Ammonium Cations) with Anionic 1D [$Fe^{III}(oxalate)Cl_2$]$^−$ Chains, *Inorg. Chem.*, 2007, **46**, 3089–3096.

36 B. Zhang, Z. Wang, H. Fujiwara, H. Kobayashi, M. Kurmoo, K. Inoue, T. Mori, S. Gao, Y. Zhang and D. Zhu, Tetrathiafulvalene [$Fe^{III}(C_2O_4)Cl_2$]: An Organic–Inorganic Hybrid Exhibiting Canted Antiferromagnetism, *Adv. Mater.*, 2005, **17**, 1988–1991.

37 B. Zhang, Z. Wang, Y. Zhang, K. Takahashi, Y. Okano, H. Cui, H. Kobayashi, K. Inoue, M. Kurmoo, F. L. Pratt and D. Zhu, Hybrid Organic-Inorganic Conductor with a Magnetic Chain Anion: κ-BETS$_2$[$Fe^{III}(C_2O_4)Cl_2$] [BETS = Bis(ethylenedithio)tetraselenafulvalene], *Inorg. Chem.*, 2006, **45**, 3275–3280.

38 D. Armentano, T. F. Mastropietro, G. De Munno, P. Rossi, F. Lloret and M. Julve, New Extended Magnetic Systems Based on Oxalate and Iron(III) Ions, *Inorg. Chem.*, 2008, **47**, 3772–3786.

39 T. F. Mastropietro, N. Marino, G. De Munno, F. Lloret, M. Julve, E. Pardo and D. Armentano, Selective Guest Inclusion in Oxalate-Based Iron(III) Magnetic Coordination Polymers, *Inorg. Chem.*, 2016, **55**, 11160–11169.

40 R. M. Silverstein, C. G. Bassler and T. C. Morrill, *Spectrometric Identification of Organic Compounds*, John Wiley & Sons, New York, 1974.

41 P. Ramaswamy, N. E. Wong, B. S. Gelfand and G. K. H. Shimizu, A Water Stable Magnesium MOF That Conducts Protons over $10^{−2}$ S $cm^{−1}$, *J. Am. Chem. Soc.*, 2015, **137**, 7640–7643.

42 W. Xia, Y. L. Wang, M. A. Silver, D. X. Gui, Z. L. Bai, Y. X. Wang, L. Wei, L. H. Chen, D. W. Juan, Z. F. Chai and S. A. Wang, Superprotonic conduction through one-dimensional ordered alkali metal ion chains in a lanthanide-organic framework, *Chem. Commun.*, 2018, **54**, 4429–4432.

43 S. M. Elahi, S. Chand, W. H. Deng, A. Pal and M. C. Das, Polycarboxylate-Templated Coordination Polymers: Role of Templates for Superprotonic Conductivities of up to 10^{-1} Scm^{-1}, *Angew. Chem., Int. Ed.*, 2018, **57**, 6662–6666.

44 S. Pili, P. Rought, D. I. Kolokolov, L. F. Lin, I. Silva, Y. Q. Chen, C. Marsh, I. P. Silverwood, V. G. Sakai, M. Li, J. J. Titman, L. Knight, L. L. Daemen, A. J. Ramirez-Cuesta, C. C. Tang, A. G. Stepanov, S. H. Yang and M. Schroder, Enhancement of Proton Conductivity in Nonporous Metal–Organic Frameworks: The Role of Framework Proton Density and Humidity, *Chem. Mater.*, 2018, **30**, 7593–7602.

45 T. Yamada, M. Sadakiyo and H. Kitagawa, High Proton Conductivity of One-Dimensional Ferrous Oxalate Dihydrate, *J. Am. Chem. Soc.*, 2009, **131**, 3144–3145.

46 O. D. Rigaku, *P.R.O. CrysAlis, version: 1.171.39.46*, Rigaku Oxford Diffraction Ltd, Yarnton, England, 2018.

47 G. M. Sheldrick, SHELXT – Integrated space-group and crystal-structure determination, *Acta Crystallogr., Sect. A: Found. Adv.*, 2015, **71**, 3–8.

48 L. J. Farrugia, WinGX and ORTEP for Windows: an update, *J. Appl. Crystallogr.*, 2012, **45**, 849–854.

49 L. Spek, Single-crystal structure validation with the program. PLATON, *J. Appl. Crystallogr.*, 2003, **36**, 7–13.

50 C. F. Macrae, I. Sovago, S. J. Cottrell, P. T. A. Galek, P. McCabe, E. Pidcock, M. Platings, G. P. Shields, J. S. Stevens, M. Towler and P. A. Wood, Mercury 4.0: from visualization to analysis, design and prediction, *J. Appl. Crystallogr.*, 2020, **53**, 226–235.

51 K. Momma and F. Izumi, VESTA 3 for three-dimensional visualization of crystal, volumetric and morphology data, *J. Appl. Crystallogr.*, 2011, **44**, 1272–1276.